Physics of Fluids

Saturated film boiling at various gravity levels under the influence of electrohydrodynamic forces

Cite as: Phys. Fluids **29**, 032104 (2017); https://doi.org/10.1063/1.4978056
Submitted: 01 October 2016 . Accepted: 22 February 2017 . Published Online: 15 March 2017

Vinod Pandey, Gautam Biswas, and Amaresh Dalal

Saturated film boiling at various gravity levels under the influence of electrohydrodynamic forces

Vinod Pandey, Gautam Biswas, and Amaresh Dalal
Department of Mechanical Engineering, Indian Institute of Technology, Guwahati 781039, India

(Received 1 October 2016; accepted 22 February 2017; published online 15 March 2017)

The present work is focused on the analyses of the bubble growth and heat transfer characteristics in saturated film boiling at various levels of gravity. In addition to this, the occurrence of self-similarity in interface structures during the bubble growth is examined. The phenomenon of bubble growth is strongly influenced by the buoyant forces due to gravity and its dominant effect is found to be replaced by the electrohydrodynamic forces in reduced gravity conditions. The decrease in gravitational acceleration results in increasing the characteristic wavelength and time scale. The bubble volume and maximum height before pinch-off thus increase enormously as the gravity value is reduced. The bubble pinch-off velocity is found to be decreased significantly in the case of reduced gravity condition. Heat transfer rate deteriorates in reduced gravity conditions which can be recovered by the externally imposed electric field. The dominance of electric field on the heat transfer rate is found to be more in reduced gravity condition. However, as the value of imposed electric field is enhanced, the difference in the effect of increasing heat flux tends to reduce. *Published by AIP Publishing.* [http://dx.doi.org/10.1063/1.4978056]

I. INTRODUCTION

Boiling and condensation have been considered as the most effective means of heat transfer in many technological applications. Due to the large difference in density of the vapour and that of the liquid phases, buoyancy force plays an important role in governing the physics of the two phase flow. Gravity is thus included in most of the empirical correlations for heat transfer in boiling. Change in gravity strongly affects the convection currents and thus the momentum and energy transport during the boiling processes. The main advantage of pool boiling in terrestrial conditions is the inevitable movement of the fluids due to buoyancy. As the gravity is reduced, the phenomenon of phase separation becomes difficult and external power is required for centrifugal or capillarity based flow separators.

Study of variable gravity effects on boiling is important in space applications. Gravity higher than the Earth's gravity (g_e) is experienced during space vehicle launch while the reduced gravity is experienced in various space applications. The space applications demand the study in microgravity or zero gravity conditions while the reduced gravity study is of significance for other terrestrial conditions like Martian or lunar atmosphere. The so far available techniques for the experimental study in low gravity are through drop towers, parabolic flights, sounding rocket flights, and orbital flights. Among these, the experiments performed using drop towers are the only ground based techniques.

All the regions in the boiling curve are differently influenced by the reduction in gravity. Studies performed by various authors provided somewhat contradictory results[1,2] for the effect of heat transfer coefficient in nucleate boiling region. The critical heat flux (CHF) value is found to decrease with the reduction in gravity. In the film boiling region, various authors found that the heat transfer coefficient decreases with the reduction in gravity owing to the decrease in bubble release frequency from the vapour film to the bulk liquid.

Many authors concluded the boiling phenomena to have a weak dependence on gravity and found negligible shift in boiling curve through the data obtained from their experiments.[2,3] Zell *et al.*[2] observed that film boiling regime is highly influenced by the variation in the level of gravity. However, the boiling curve is negligibly affected due to change in gravity in the nucleate boiling regime. An increase in the diameter of bubbles was observed in the case of nucleate boiling though. The experiments on boiling are highly sensitive to the heater geometry, surface roughness, liquid subcooling, or liquid pressure. Oka *et al.*[1] observed a significant deterioration in heat transfer in the low heat flux nucleate boiling for water while there was only a slight change in heat transfer due to reduced gravity for the organic liquids (CFC-113 and n-pentane). Lienhard[4] pointed out that nucleate boiling in the regime of isolated bubbles is gravity dependent while it is gravity independent in the slugs and column regime of nucleate boiling. Moissis and Berenson[5] provided a correlation for the transition heat flux in the former case of isolated bubbles, i.e.,

$$q_{(MB)} = 0.11\rho_v h_{lv}(\sigma g/(\rho_l - \rho_v))^{1/4}\beta^{1/2}. \quad (1)$$

Here, ρ is the density of the medium, σ is the surface tension coefficient, β is the contact angle, and h_{lv} is the latent heat of evaporation. The suffixes l and v refer to the liquid and vapour phase, respectively. While referring to the above correlation, Lienhard[4] gave the correlation for peak heat flux independent of gravity in the slugs and column regime of nucleate boiling as

$$q_{max} = \rho_v h_{lv} u_c (A_j/A_h), \quad (2)$$

where A_j is the cross-sectional area of jets, A_h is the heater area, and u_c is the vapour velocity in the jets.

The initial studies of the influence of gravity on boiling phenomena can be attributed to the pioneering work by Siegel and co-workers.[6–8] Through the drop towers experiments, they performed various sets of experiments at various values of reduced gravity field mostly in the nucleate boiling range. Larger bubble diameter, decrease in bubble departure velocity, and decreased critical heat flux as the gravity is reduced were some of the conclusions of their experimental investigations. Contrary to their expectations for the decrease in heat flux in reduced gravity, they observed a significantly comparable value of heat flux with that at normal gravity. This is attributed to the turbulence generated due to the merger of the smaller bubbles with the already formed large primary bubble.

Merte and Clark[9] also performed the experiments on fractional gravity and concluded that the heat transfer coefficient in the film boiling region is proportional to $(1/4)^{\text{th}}$ power of the fractional gravity. The same proportionality holds for the maximum and the minimum heat flux values. Lee *et al.*[10] observed an increase in heat transfer coefficient and significant decrease in maximum heat flux with decreasing gravity in the nucleate boiling regime. They also anticipated the reduction in minimum heat flux value. The heat transfer coefficient is found to be slightly dependent on the degree of subcooling. The heat transfer was governed by the formation of a static large bubble over the surface and the merging of the nearby neighbouring bubbles with the larger static bubble.

Unlike the observations of Lee *et al.*,[10] Kim and Benton[11] observed the formation of a larger bubble over the heated surface but it kept on moving over the heater area affecting the heat transfer rate. Heat fluxes obtained in low gravity and high gravity were observed to be greater than that at Earth's gravity. Raj *et al.*[12] also performed experiments in the gravity range from 0 to 1.8 times of Earth's gravity. They explained the phenomena by differentiating the results in two regimes. First, the low gravity regime where large primary non-departing bubbles are formed, and second, high gravity regime where small bubbles continuously depart from the surface. Heat flux is more dependent on the low gravity regime as compared to that of the high gravity regime.

The dominant mechanism controlling the dynamics of bubble growth during boiling in low gravity is still a subject of debate. Straub and co-workers[13–15] emphasized on the effect of thermocapillary convection currents due to the temperature gradient along the interface of the growing bubble. They showed from their experimental and numerical results, the influence of the surface tension force on the heat transfer characteristics of the boiling phenomena. The thermocapillary convection currents resulted in the lateral motion of the bubbles and their merger which maintained the turbulent motion of the detached bubbles. The heat transfer rate in low gravity was found to be equivalent to that in the terrestrial normal gravity condition. They also concluded that the heat transfer reduces significantly in the transition and film boiling regime while it is slightly affected in the nucleate boiling regime. Shatto and Peterson[16] also emphasized on the effect of thermocapillary convection on boiling phenomena.

Qiu and Dhir[17] showed the dynamics of bubble growth during nucleate boiling from bubble inception to lift-off in the low gravity environment of parabolic flight. Bubble departure diameter (D_d) was found to be related to the gravity level obeying $D_d \propto 1/\sqrt{g}$. In the case of multiple bubble lift-off after merger, the equivalent diameter was found to be smaller than that of the single bubble at the same gravity level. Abarajith *et al.*[18] studied the effect of gravity on bubble departure diameter using numerical simulations and showed the same scaling as was observed experimentally by Qiu and Dhir.[17] Although, they showed the dependence on contact angle on the scaling between departure diameter and gravity.

A series of experiments on nucleate boiling was performed in the International Space Station (ISS) by Dhir and co-workers.[19–21] The experimental work was performed following the numerical simulation[20] of single and multiple bubbles in nucleate boiling determining the spacing between the prefabricated heat transfer zones. Experiment was performed in the subcooled and saturated conditions in the microgravity and was compared with the results obtained owing to the Earth's gravity. The effect of non-condensable gases was also considered which resulted in local pressure drop at the interface. In the lower heat flux range, lateral bubble merger leads to a single larger bubble which lifts-off as the heat flux is increased. Normalized heat transfer coefficients were found to be weakly dependent on gravity.

Wan and Zhao[22] observed slight enhancement in heat transfer in the low gravity in experiments using R113 as fluid with a wire heater while a decrease in heat transfer with plate heater using F72 as fluid. Zhao *et al.*[23] observed abrupt transition to film boiling from nucleate boiling under the low gravity condition. A decrease in CHF with reducing gravity was also observed.

Verplaetsen and Berghmans[24,25] studied the effect of electric field on bubble morphology during boiling and observed a tremendous increase in heat transfer coefficient with the application of electric field. Di Marco and Grassi[26] focused on the pool boiling with applied external electric field under low gravity conditions generated through parabolic flights. In the nucleate boiling regime, the effect of both electric field and gravity was mentioned to be negligible.[27] In reduced gravity, the critical heat flux and the heat transfer coefficient in the film boiling regime were appreciably deteriorated. However, both of these were recovered and enhanced with the application of electric field. The electrohydrodynamic (EHD) enhancement of heat transfer during film boiling was observed on both Earth's gravity and reduced gravity conditions. At a very high value of electric field, the value of critical heat flux becomes almost indistinguishable on both low gravity and Earth's gravity conditions. However, the relative increase in critical heat fluxes as compared to their corresponding values with zero EHD is more in the case of low gravity. The results obtained for the ratio of critical heat flux with electric field to that without electric field were in agreement with the corresponding ratio derived from the hydrodynamic theory by Johnson[28] as

$$\frac{q_{(CHF,E)}}{q_{(CHF,0)}} = \sqrt{\frac{El^* + \sqrt{El^{*2} + 3}}{\sqrt{3}}}, \tag{3}$$

where $El^* = \frac{f(E,\epsilon_l,\epsilon_v)}{\sqrt{(\rho_l-\rho_v)\sigma g}}$ and $f(E,\epsilon_l,\epsilon_v) = \frac{\epsilon_l(\epsilon_l-\epsilon_v)^2}{\epsilon_v(\epsilon_l+\epsilon_v)}\epsilon_0 E_l^2 = \frac{\epsilon_v(\epsilon_l-\epsilon_v)^2}{\epsilon_l(\epsilon_l+\epsilon_v)}\epsilon_0 E_v^2$. Here E_l is the strength of electric field in the liquid phase and E_v is the strength of electric field in the vapour phase. Also

$$\frac{\lambda_E}{\lambda_0} = \frac{\sqrt{3}}{El^* + \sqrt{El^{*2}+3}}, \tag{4}$$

where λ_E is the wavelength (distance between two adjacent bubbles) in the presence of an electric field and λ_0 is the wavelength without electric field. Johnson[28] predicted the ratio of heat flux with electric field, $q(E)$, to heat flux without electric field, $q(0)$, in the film boiling regime as

$$\frac{q(E)}{q(0)} = \left[1 + \frac{f}{3\left[\frac{4}{3}(\rho_l-\rho_v)g\sigma\right]^{1/2}}\right]^{1/2}. \tag{5}$$

The subscripts E and 0 refer to the value with electric field and value without electric field, respectively. The electric influence number (El^*) is a function of dielectric permittivities (ϵ) of the media and the electric field strength. Carrica *et al.*[27] performed experiments using R113 in the film boiling regime to determine the changes in bubble release frequency and wavelengths under the influence of electric field. The most important feature from their results is the clear evidence of boiling-transition within the film boiling regime with the application of electric field. At lower superheat, the electric field increases the bubble release frequency with the significant decrease in wavelength. At this stage, there is no dominant wavelength indicating the bubble spacing. With further increase in wall superheat, the effect of electric field gets suppressed and bubbles again start to depart with larger diameter and increased dominant wavelength.

Di Marco *et al.*[29] found the similar transition in low gravity film boiling with the effect of electric field. The film boiling was found to be very sensitive to the gravity level at low intensity of electric field while it was insensitive to the gravity level at very high intensity of electric field value. In addition to the above mentioned researchers, Markels and Durfee,[30] Lovenguth and Hanesian,[31] and Cooper[32] have also studied the effect of electric field on boiling phenomena.

Numerical simulation of the boiling phenomena was initiated by Son and Dhir[33] with water at 1 atm pressure and later near critical pressure.[34] Interface was captured using the level-set technique. Using the combined level-set and volume of fluid (CLSVOF) approach,[35] Tomar *et al.*[36] simulated the single bubble growth in film boiling using water and R134a as working fluids and showed the effect of superheat on bubble dynamics and heat transfer characteristics. The work was later extended to study multimode bubble formation[37] and the transition of instability modes from Rayleigh-Taylor to Taylor-Helmholtz owing to increased superheat. This can be attributed to the increase in magnitude of the dominant wavelength which defines the spacing between adjacent bubbles.[38]

Welch and Biswas[39] showed the effect of EHD on the film boiling. A decrease in the most dominant wavelength and increase in Nusselt number were observed with the application of electric field. Later, Tomar *et al.*[40] observed the increase in bubble release frequency with the application of electric field and a significant decrease in bubble spacing in the same domain was also observed. The formulation for the electric force term was followed from Tomar *et al.*[41] Using the same formulation, Pandey *et al.*[42] have showed the effect of different intensities of electric field and superheat on the bubble release frequency and the bubble spacing. It was showed that the maximum height of the bubbles remains almost constant even after the application of electric field at any specified value of superheat. The heat transfer analysis was performed and compared with the analytical expression for the ratio of heat flux with electric field to heat flux without electric field given by Johnson.[28] The comparative influence of electric field on heat transfer rate at lower superheat was found to be more than that at higher superheat for the same intensity of electric field.

The study concerning the effect of low gravity in film boiling has remained a topic of substantial interest. The present study is focused to analyze, in detail, the changes in bubble dynamics, spacing between the adjacent bubbles, and heat transfer characteristics at various range of gravity levels. Attempts have been made to determine the changes in the maximum height of the bubbles, radius of the bubble, and the bubble pinch-off velocity with change in level of gravity. The changes in bubble morphology with the introduction of electric field in both normal and reduced gravity conditions have been explored. Further, it has been tried to show the increase in dominating effect of electric field with the reduction in gravity level. In addition to this primary focus of the paper, we have also tried to show the self-similarity behaviour of the bubble interface during its linear growth phase.

II. FORMULATION

A. Governing equations

Applying the CLSVOF algorithm for the interface capturing, the present study considered initially a thin vapour film over a heated surface under a liquid pool. Using the single fluid formulation and considering the fluids to be incompressible, the final form of momentum equation which is solved is given by

$$\rho(\alpha)\left[\mathbf{U}_t + \nabla\cdot(\mathbf{UU})\right] = -\nabla p + \rho(\alpha)\mathbf{g} + \nabla\cdot(2\mu(\alpha)\mathbf{D}_v) + \sigma\kappa\hat{\mathbf{n}}\delta_s + \mathbf{f}_v^{\mathrm{E}}, \tag{6}$$

where α is the volume fraction of liquid given by $(\rho-\rho_v)/(\rho_l-\rho_v)$. $\mathbf{U}$ is the velocity vector and $\mathbf{D}_v = (\nabla\mathbf{U}+\nabla\mathbf{U}^{\mathbf{T}})/2$ is the rate of deformation tensor. The density, $\rho(\alpha)$, and viscosity $\mu(\alpha)$ are the volume fraction based density and viscosity, respectively.[38] The fourth term on the right hand side represents the surface tension force based on the model formulated by Brackbill *et al.*[43] The normal vector and the curvature at the interface in each two phase cell are calculated based on the smoothed void fraction. The smoothed void fraction is defined on the basis of Heaviside function.[44]

The last term on the right hand side of Eq. (6) represents the electric force term derived from the Maxwell's stress tensor($\boldsymbol{\tau}^{\mathrm{E}}$). It is given as

$$\mathbf{f}_v^{\mathrm{E}} = \nabla\cdot\boldsymbol{\tau}^{\mathrm{E}} = -\frac{1}{2}E^2\nabla\epsilon_0\epsilon, \tag{7}$$

TABLE I. Properties of water at near critical pressure ($P_r = P/P_{sat} = 0.99$).

T_{sat} = 646 K; P_{sat} = 21.9 MPa; h_{lv} = 276.4 kJ/kg; σ = 0.07 mN/m					
Phase	Density(ρ) (kg/m^3)	Viscosity(μ) (μN s/m^2)	Conductivity(k) (W/mK)	Specific heat(c_p) (kJ/kg K)	Rel. permittivity (ϵ)
Liquid	402.4	46.7	0.5454	2.18 ×10^2	7.35
Vapour	242.7	32.38	0.5383	3.52 ×10^2	3.71

TABLE II. Properties of R134a at near critical pressure ($P_r = P/P_{sat} = 0.92$).

T_{sat} = 370.46 K; P_{sat} = 3.763 MPa; h_{lv} = 54.6 kJ/kg; σ = 0.182 mN/m					
Phase	Density(ρ) (kg/m^3)	Viscosity(μ) (μN s/m^2)	Conductivity(k) (W/mK)	Specific heat(c_p) (kJ/kg K)	Rel. permittivity (ϵ)
Liquid	730.8	56.72	0.0520	5.128	5.0
Vapour	301.9	21.71	0.0415	4.445	4.2

where E is the electric field. The electric force is defined considering the medium to be perfectly dielectric in the absence of free charge. The model is mentioned in detail by Pandey *et al.*[42] The electric force formulation and discretization are available in the work of Tomar *et al.*[41] The electric potential equation is given by

$$\nabla \cdot (\epsilon \epsilon_0 \nabla \psi) = 0, \tag{8}$$

where ϵ is the relative dielectric permittivity of the medium and ϵ_0 is the absolute dielectric permittivity of vacuum. The electric potential function is ψ.

The interface and bulk liquid are considered to be at constant temperature throughout the simulation and the energy equation in the vapour region is given as

$$\frac{\partial T}{\partial t} + \mathbf{U} \cdot \nabla T = \frac{k_v}{\rho c_p} \nabla^2 T, \tag{9}$$

where T is the temperature, k_v is the thermal conductivity of the vapour phase, and c_p is the specific heat of the vapour phase.

The mass conservation equation for the bulk vapour and liquid region is given by

$$\nabla \cdot \mathbf{U} = 0. \tag{10}$$

Equation (10) is valid only in the bulk liquid and vapour cells. In the two-phase cells, the heat flux from vapour to liquid leads to vapour generation and hence there is a jump in mass and velocity at the interface.[42] The modified continuity equation considering the mass jump across the interface is given by

$$\int_{S_C} \mathrm{U} \cdot \mathrm{n} dS + \int_{S_I(t)} \left(\frac{1}{\rho_l} - \frac{1}{\rho_g} \right) \frac{|\mathrm{q}| \cdot \mathrm{n}}{h_{lg}} dS = 0, \tag{11}$$

where $S_I(t)$ is the interface area, S_c is the cell surface area, and q is the heat flux across the interface.[45,46]

B. Boundary conditions

The simulations are performed for various domain lengths proportional to the Berenson's most dominant wavelength,[47] $\lambda_{\mathbf{B}} = 2\pi\sqrt{3\sigma/(\rho_l - \rho_v)\mathbf{g}}$. The fluids used are water and R134a near critical pressure whose properties have been mentioned in Tables I and II, respectively. Symmetry conditions are provided at the left and right boundaries of the simulation domain (Fig. 1) as

At $x = 0$ (left boundary) and $x = L$ (right boundary),

$$u = 0, \frac{\partial v}{\partial x} = 0, \frac{\partial T}{\partial x} = 0, \frac{\partial F}{\partial x} = 0, \frac{\partial \phi}{\partial x} = 0, \frac{\partial \psi}{\partial x} = 0. \tag{12}$$

Outflow condition is incorporated at the top boundary and no-slip wall condition at the bottom boundary. The bottom wall is explicitly defined at a constant temperature. The conditions are mentioned as follows:

At $y = H$ (top boundary),

$$\frac{\partial u}{\partial y} = \frac{\partial v}{\partial y} = \frac{\partial T}{\partial y} = \frac{\partial F}{\partial y} = \frac{\partial \phi}{\partial y} = 0, \quad P = P_0 \tag{13}$$

and at $y = 0$ (bottom boundary),

$$u = v = 0 \text{ and } T = T_{sat} + \Delta T_{sup}. \tag{14}$$

Here, P_0 is the saturation pressure less the hydrostatic pressure difference from the vapour film to the top boundary of the domain.

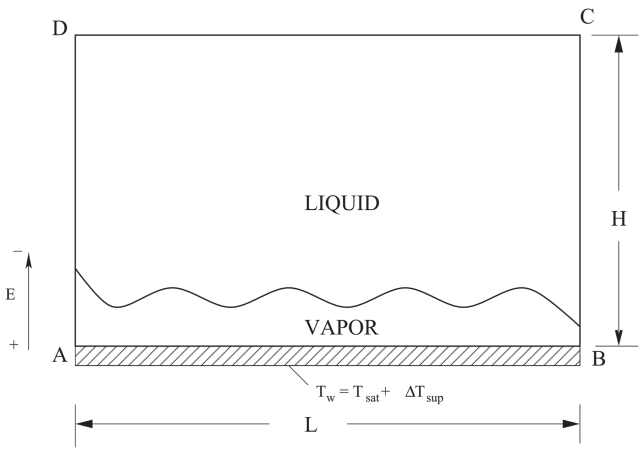

FIG. 1. Schematic of the computational domain.

III. NUMERICAL PROCEDURE

The numerical simulation is initiated by considering a thin film of vapour above the bottom boundary of the domain. A random perturbation is given to the vapour film along horizontal direction. Temperature in the liquid phase and at the interface is considered at a constant saturation temperature (T_{sat}). A staggered grid arrangement is followed for the spatial discretization of governing equations. The energy Equation (9) is solved implicitly where the convection terms are discretized following QUICK scheme.[48] The updated temperature distribution is used to calculate the heat flux at the interface. The modified continuity equation which is solved in the two-phase cells utilizes the interfacial heat flux to calculate the jump in mass and velocity. The discrete momentum equation determines the updated velocity which further determines the updated pressure values by solving the pressure equation. The pressure and electric potential equations are solved using HYPRE multigrid solver.

There is a continuous vapour generation at the interface due to heat transfer from the vapour to liquid region. The interface, therefore, needs to be advected with time by solving the advection equation for void fraction and level-set function given by

$$\frac{\partial \alpha}{\partial t} + \mathbf{U} \cdot \nabla \alpha = 0 \tag{15}$$

and

$$\frac{\partial \phi}{\partial t} + \mathbf{U} \cdot \nabla \phi = 0, \tag{16}$$

respectively. A coupled second order operator split approach[49] is followed for solving the advection equation. The detailed procedure for solving the advection equation has been mentioned in the work of Tomar *et al.*[37] The level-set function is defined as the signed distance function from the interface (positive on the liquid side and negative on the vapour side). The convective terms in the momentum, advection, and level-set equations are discretized using ENO (Essentially Non-Oscillatory) scheme as described in Chang *et al.*[50]

The thickness of the interface is determined by the Heaviside function which depends on the values of level-set function at each cell within the interface thickness. The interface thickness in the present simulations is equivalent to three times of the grid spacing across every two-phase cell. The definition of the Heaviside function and details of the CLSVOF algorithm can be found in the work of Tomar *et al.*[40]

IV. RESULTS AND DISCUSSION

Boiling beyond critical heat flux region, i.e., film boiling is simulated using the model and boundary conditions as mentioned in Sec. II. It is to be noted that the length scale $l_s = \sqrt{\sigma/(\rho_l - \rho_v)g}$ is a function of gravity. The most dangerous wavelength in Earth's normal gravity near critical pressure for water ($P = 0.99P_c$) is $\lambda_B = 0.002\,275$ m and for R134a ($P = 0.92Pc$) is $\lambda_B = 0.002\,263$ m. The grid dimension is taken as $\Delta x = \lambda_B/240$ in all the simulations performed where λ_B corresponds to the most dangerous wavelength in terrestrial condition. A time step of value $\Delta t = 5.0 \times 10^{-6}$ s is used in all simulations which is consistent with the capillary time limit. The bubble dimensions and spacing between adjacent bubbles are expected to be enhanced in the case of reduced gravity as compared to those due to normal gravity condition. Simulations have been performed considering saturated water and refrigerant R134a as working fluids near critical pressure. In order to analyze the variation in bubble release pattern and the shape of the bubble under normal and reduced gravity conditions, numerical simulations have been performed with and without the application of an electric field. In Secs. IV A and IV B, we tried to explore the effect of variation in gravity level on the bubble dynamics, i.e., the bubble release frequency and spacing between bubble formation sites, pinch-off velocity, bubble release time, and the maximum height of bubble. In addition to these, the changes in heat transfer characteristics owing to different levels of gravity and various intensities of electric field have been determined using the simulations. Together with the Earth's normal gravity, two different gravity levels have been considered in the present study. In order to compare with some realistic values, we considered gravity levels corresponding to the moon ($g/g_e = 0.16$) and Mars ($g/g_e = 0.37$).

A. Boiling at different levels of gravity

During film boiling, the heating of the vapour layer from the superheated bottom surface leads to vapourization of the adjacent liquid mass close to the interface. The vapour mass generated continuously tends to buoy away due to the difference in density of vapour and liquid. The tendency of movement of vapour mass gets suppressed as the gravity is reduced. Simulations are performed in the domain size with horizontal span of $5\lambda_B$ for R134a and $3\lambda_B$ for water to show the change in bubble morphology. It may be mentioned that the bubble pinch-off and the frequency of bubble release have been accurately predicted using a similar domain and technique as by Agarwal *et al.*[46] The vertical span varies as the wavelength corresponding to the gravity-level of interest.

In order to determine the morphological variations at the interface owing to varying gravity-levels, simulations have been performed in the domain size of $5\lambda_B$ for R134a. It can be observed from Fig. 2 that the dimensions of the bubbles become larger as the gravity is reduced. The spacing between adjacent bubble formation sites increases significantly with the reduction in the level of gravity. Also, the time for the first set of bubble departure increases with the decrease in gravity. The time for the first set of bubble release corresponding to each gravity-level is illustrated in Fig. 2. The number of bubbles

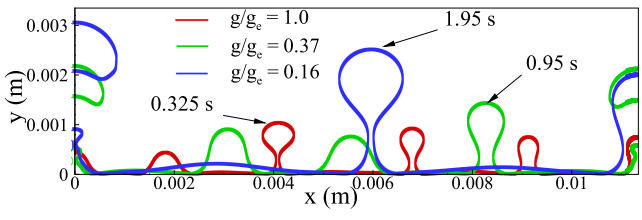

FIG. 2. Comparison of interface profile at the instant of first set of bubble release at three different levels of gravity for R134a with $\Delta T = 20$ K.

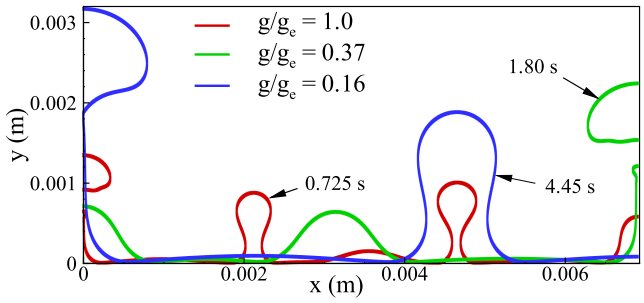

FIG. 3. Comparison of interface profile at the instant of first set of bubble release at three different levels of gravity for water with $\Delta T = 5$ K.

for a fixed domain at any given gravity-level should be consistent with the critical wavelength defined by Taylor-Helmholtz instability. The number of bubbles for the case of $g/g_e = 1.0$ is five which is consistent with the requirements of Taylor-Helmholtz instability. For $g/g_e = 0.37$ the number reduces to four bubbles, for which the number of bubbles defined by instability criterion is between three and four. For $g/g_e = 0.16$, two bubbles in $5\lambda_B$ domain is also consistent with the instability criterion for that level of gravity.

Similar analysis has been performed using water as the working fluid in the domain size of $3\lambda_B$. The results are shown in Fig. 3 for the first set of bubble release. Increase in bubble size and increased distance between bubble formation sites are observed at reduced gravity conditions.

In order to show the variation in bubble dynamics as a result of change in the level of gravity, a minimum domain length is required. The larger domain length explains the variations in a better manner. As compared to the case of water, the domain length in the case of R134a can be extended to $5\lambda_B$ due to the low values of specific heat and latent heat of vapourisation.

Fig. 4 shows the variation in the height of the apex of the vapour bubble with time for both normal ($g/g_e = 1.0$) and reduced gravity ($g/g_e = 0.1$) conditions during the growth of a single bubble. It can be clearly observed that the maximum height of the bubble in reduced gravity is more than three times of the one in normal gravity. The number of bubbles formed (number of peaks) is five for normal gravity as compared to the single bubble formed in reduced gravity during the same time interval. The rate of increase of the maximum height of

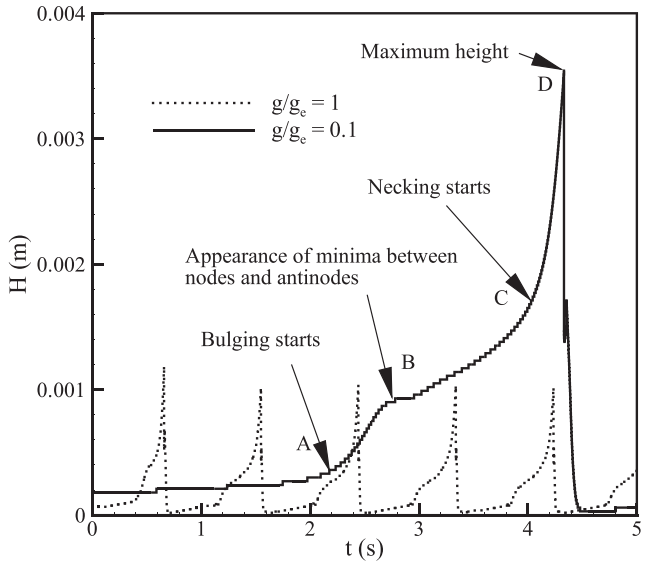

FIG. 4. Variation of apex height of bubble with time at normal and reduced gravity conditions for water at $\Delta T = 5$ K.

interface till the onset of bulging of the bubble is very low as compared to the growth rate after neck formation. It may be stated that along with the slower growth of interface due to reduced gravity, the bubble volume also requires to be larger so that the bubble can generate enough buoyancy force to be buoyed away. The larger bubble volume is indicated by greater apex height of the bubble.

The decrease in buoyancy force due to the reduced gravity results in slower rate of bubble growth. It is clearly illustrated in Fig. 4 where the slow growth rate leads to the delayed departure of the bubble in the case of reduced gravity. The reduction in buoyancy force not only leads to the delay in bubble departure but also can be contemplated to reduce the bubble pinch-off velocity from the vapour film. This effect is verified from the plot of the vertical velocity of the vapour bubble during its growth period starting from its inception to the departure. This is illustrated in Fig. 5 where the vertical velocity is averaged over all the vapour cells and two phase cells associated with the growing vapour bubble. The velocity is calculated after the vapour bulge attains a height of $\lambda_B/8$. As can be observed from the plot, the maximum velocity occurs just before the bubble roll-up (mushroom shape) begins. Specifically, this is

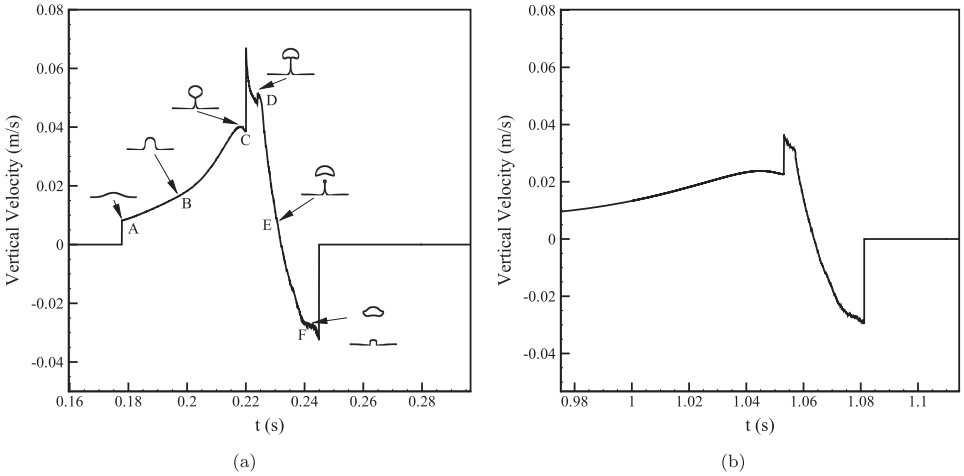

FIG. 5. Variation in vertical velocity during the growth of bubble in (a) normal gravity ($g/g_e = 1.0$) and (b) reduced gravity ($g/g_e = 0.16$) with time for R134a at $\Delta T = 30$ K.

the instant of having the neck stretched before the pinch-off. Due to the roll-up of vapour column, vortices are generated and hence some components of velocities are directed in the negative y direction. As a result, there are fluctuations in the plot near the maximum value. The different shapes of bubble during its growth have been shown at the corresponding points in the plot. Point "C" corresponds to the instant just before the initiation of stretching due to neck formation. After the bubble pinch-off, the left-over vapour packet recoils back and impinges on the horizontal vapour film. This attributes to the negative velocity in the plot.

The effect of reduced gravity results in decreasing the pinch-off velocity of bubble. It can be observed from the plot that the value of pinch-off velocity at normal gravity (g/g_e = 1.0) is close to 0.05 m/s while at the reduced gravity (g/g_e = 0.16), the value decreases to about 0.03 m/s. Hence, a significant decrease in the pinch-off velocity occurs due to the reduction in gravity.

The radius of the growing bubble is also calculated using the same approach of area averaging. The area-average-based radius from all the two phase cells and vapour cells is plotted in Fig. 6 at normal and reduced gravity conditions. The plot shows that the maximum radius (≈0.066 cm) of the bubble before detachment in reduced gravity condition is more than two times the radius (≈0.032 cm) in normal gravity condition. Also the inception time and the total time of growth of the bubble are more in the case of reduced gravity as compared to that in normal gravity.

During film boiling, heat removal from the heated surface occurs as a result of the continuous departure of vapour bubbles from the vapour film to the bulk liquid. Thus the heat transfer takes place from the surface to the bulk liquid through the vapour layer. This vapour removal rate tends to decrease when the gravity is reduced. Heat transfer analysis is performed using water and R134a as the fluids, to determine the effect of variation in gravity levels. The variations in heat flux are shown in Fig. 7(a) for water and in Fig. 7(b) for R134a at different levels of gravity. For water at normal gravity (g/g_e = 1.0), the value of heat flux, averaged over space and time, is 66 kW/m^2 while it is 42 kW/m^2 at g/g_e = 0.37 and 30 kW/m^2 at g/g_e = 0.16. For R134a at normal gravity (g/g_e = 1.0), the

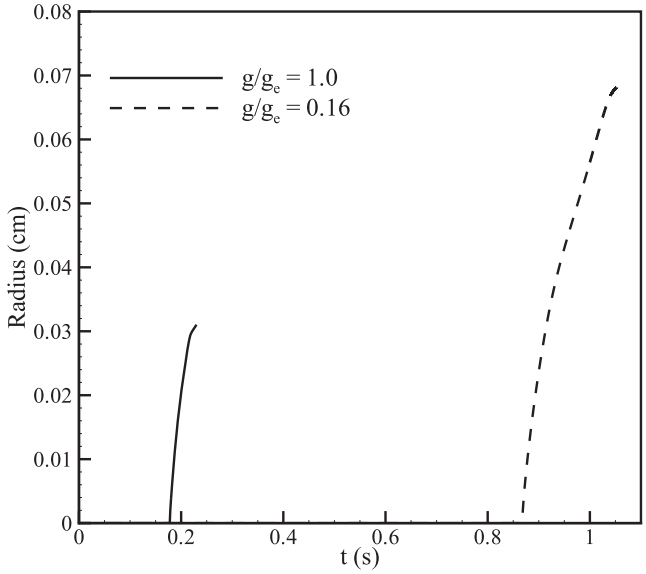

FIG. 6. Comparison of bubble radius between normal gravity (g/g_e = 1.0) and reduced gravity (g/g_e = 0.16) for R134a at ΔT = 30 K.

value of heat flux averaged over space and time is 28 kW/m^2 while it is 19 kW/m^2 at g/g_e = 0.37 and 13 kW/m^2 at g/g_e = 0.16. It is thus inferred from the heat flux results that the reducing gravity has diminishing effect on the heat transfer rate. A similar trend was observed by Zell *et al.*[2] and Merte and Clark[9] in their experimental investigations.

B. Boiling with EHD at different levels of gravity

Application of electric field along the direction of evolving vapour bubbles results in increased instabilities at the liquid-vapour interface. This can be deduced from the analytical dispersion relation for the frequency of bubble release given by Johnson.[28] The additional stresses due to electric field bring about critical morphological changes in the interface which affect the entire boiling regime. Di Marco and Grassi[26] described the existence of two different regimes of film boiling in reduced gravity under applied electric field. This was done based on the intensity of the applied electric field. At

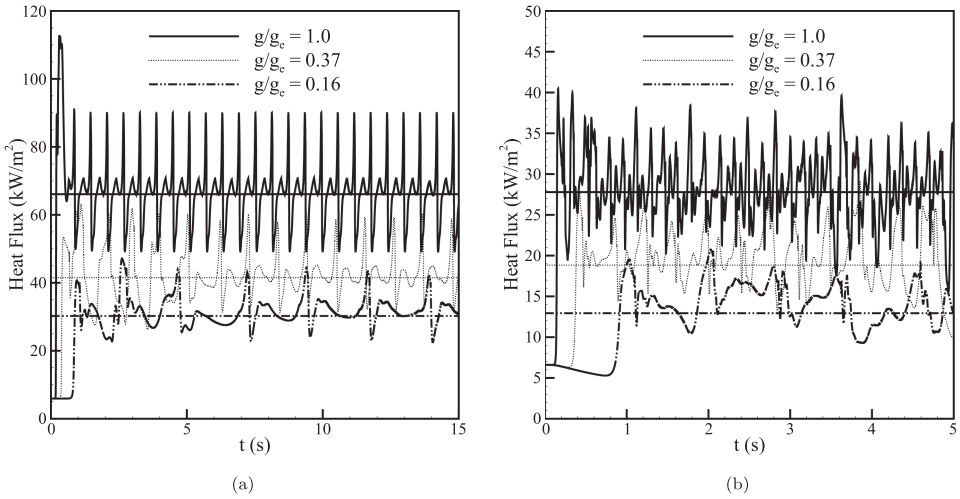

FIG. 7. Comparison of heat flux variation with time at different levels of gravity for (a) water at ΔT = 5 K and (b) R134a at ΔT = 30 K.

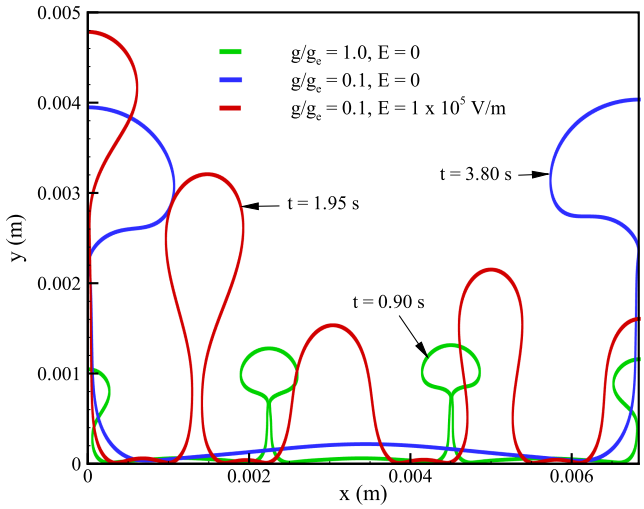

FIG. 8. Comparison of interface profile at the instant of first set of bubble release for water with ΔT = 18 K.

a low intensity of electric field under a low gravity condition, the boiling is highly affected and is deteriorated as compared to that at a normal gravity with same value of the electric field. While at a very high intensity, the difference in the effect of electric field on boiling at a low gravity and under normal gravity is not significant. Hence, beyond a certain value, electric field force dominates the flow behaviour offsetting the effect of gravity.

The increased disturbance at the interface due to the applied electric field decreases the value of the most dominant wavelength. The spacing between the adjacent bubbles decreases significantly and the bubble release frequency also gets enhanced. The effect of reduced gravity can thus be counterweighed by the application of electric field. The length and time scale in normal gravity can also be restored and controlled

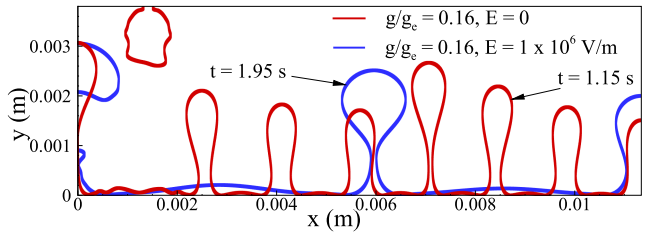

FIG. 9. Effect of an applied electric field on bubble morphology for R134a with ΔT = 20 K.

by applying a suitable intensity of electric field under reduced gravity conditions. These effects can be seen from the comparisons of the first set of bubble release at different gravity levels followed by the application of electric field at a reduced gravity, as shown in Figs. 8 and 9. Figure 8 corresponds to the simulation for water in a $3\lambda_B$ domain and Fig. 9 corresponds to that for R134a in a $5\lambda_B$ domain. The increased frequency of bubble release and reduced spacing between adjacent bubbles are observed in both fluids (water and R134a) owing to the application of electric field.

Application of electric field of the same intensity in normal and reduced gravity shows different effects. This may be contemplated from Eq. (5) which refers that as the gravity is reduced, the ratio of heat transfer with electric field to that without electric field increases. Hence, one can also speculate the change in morphological behaviour of the interface with the application of the same intensity of electric field under different levels of gravity. This may become more clear from the results shown in Figs. 10 and 11. Figure 10(a) shows discrete bubble release under normal gravity (g/g_e = 1.0) with three bubbles in $3\lambda_B$ domain. With the introduction of electric field of intensity 2×10^5 V/m, the number of bubbles increases to ten bubbles in $3\lambda_B$ domain [Fig. 10(b)]. Even under such

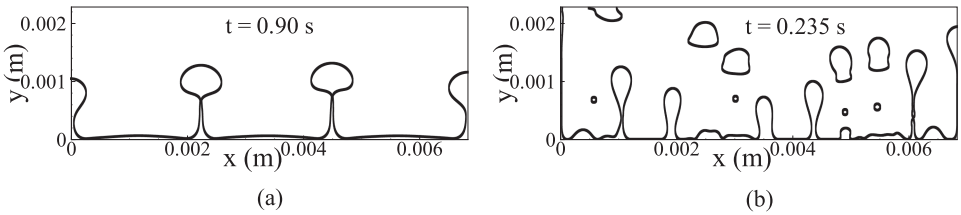

FIG. 10. Interface morphology at the instant of first set of bubble release at normal gravity (g/g_e = 1.0) (a) without electric field and (b) with an applied electric field of intensity E = 2×10^5 V/m for water with ΔT = 18 K.

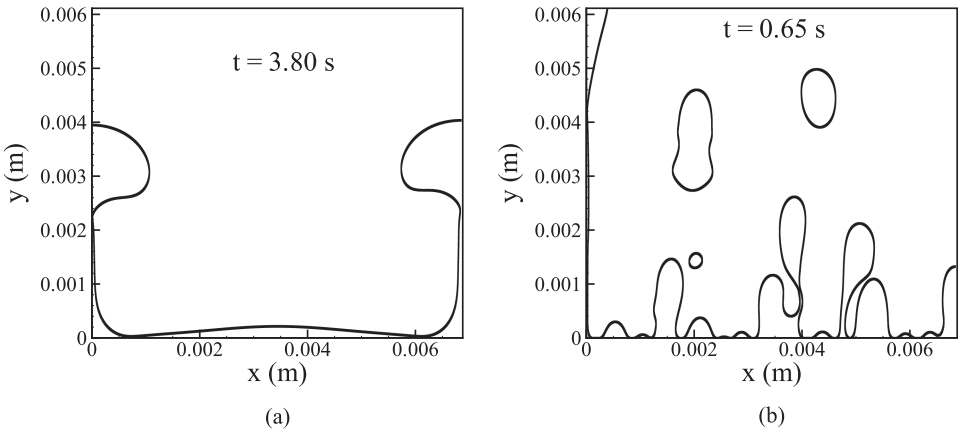

FIG. 11. Interface morphology at the instant of first set of bubble release at low gravity (g/g_e = 0.1) (a) without electric field and (b) with an applied electric field of intensity 2×10^5 V/m for water with ΔT = 18 K.

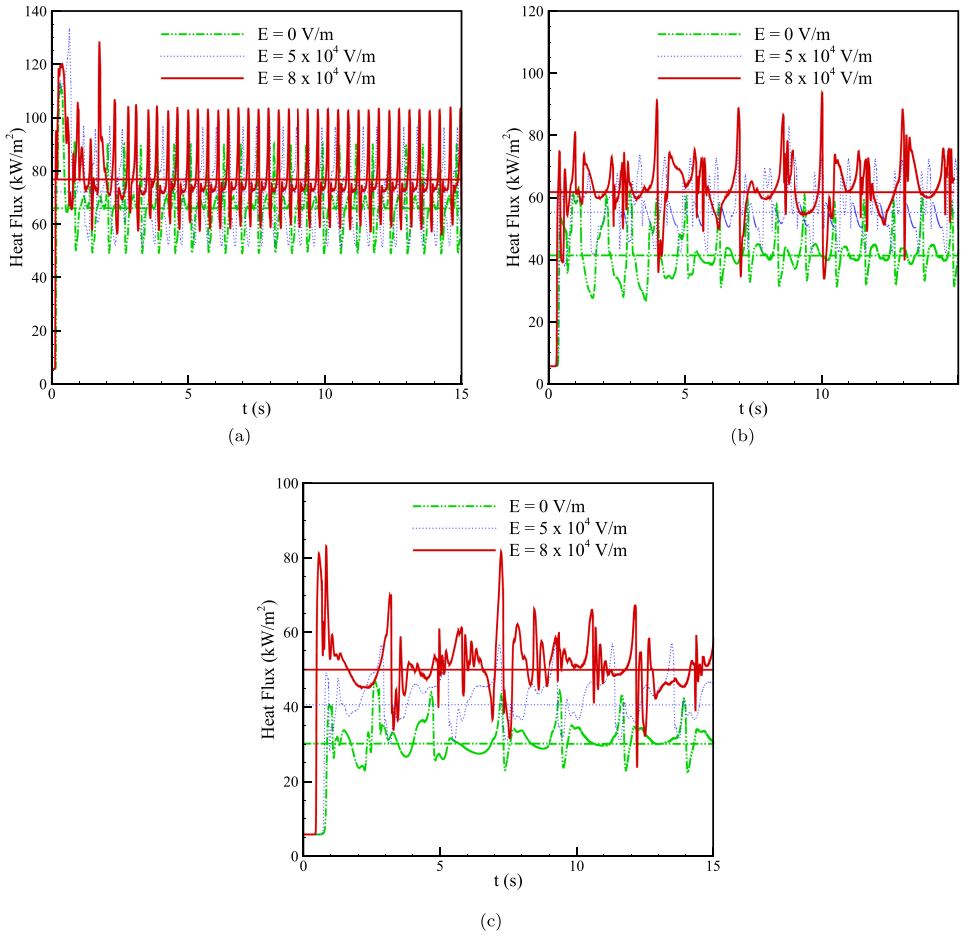

FIG. 12. Heat transfer characteristics for water at 5 K wall superheat with different values of applied electric field intensity at gravity levels of (a) g/g_e = 1.0, (b) g/g_e = 0.37, and (c) g/g_e = 0.16.

a situation, separate bubble release sites are discerned without any merger between the adjacent bubbles. The time instant of the first set of bubble release has also been shown. In the reduced gravity condition ($g/g_e = 0.1$), the bubbles detach separately [Fig. 11(a)] with a distance of $3\lambda_B$ between the adjacent bubble formation sites. However with the application of electric field, the bubble formation sites increase and the departing bubbles seem to interact vigorously and start merging with each other. The results have been shown in Fig. 11(b). The lateral merging can be due to the increased dominance of capillary forces as compared to the buoyancy force. This effect gets enhanced in reduced gravity.

The reduced gravity effect delays the departure of the bubbles from the vapour film and thus the heat transfer rate from the heated surface gets deteriorated. As the application of electric field enhances the frequency of bubble release, the heat transfer rate also gets improved. This can be observed from Figs. 12(a)–12(c) where the variation of heat flux with time is shown for different values of electric field at g/g_e = 1.0, g/g_e = 0.37, and g/g_e = 0.16, respectively. It is observed that the effect of electric field, i.e., the percentage increase in heat flux value for the same intensity of electric field, is more in reduced gravity than that of the normal gravity condition. The observed changes are tabulated in Table III. The percentage increase in heat flux owing to any imposed electric field is with respect to the value of heat flux without electric field. It can be observed from the tabulated data that the percentage increase in the heat flux for any given value of electric field increases with decrease in the level of gravity.

From the variation of heat flux with varying imposed electric field at a given value of gravity, it is observed that the effect of electric field increases with decrease in gravity. The difference in percentage increase of heat flux with the application of electric force increases with the intensity of electric field. This observation can be more clearly stated from the plots shown in Figs. 13(a) and 13(b). The heat flux plots at different levels

TABLE III. Comparison of variation in heat flux with applied electric field at various gravity levels for water.

Gravity level	q_0	$E = 5 \times 10^4$ V/m		$E = 8 \times 10^4$ V/m	
(g/g_e)	(kW/m^2)	q_E(kW/m^2)	Percentage increase (%)	q_E(kW/m^2)	Percentage increase (%)
1.0	66	72	9.0	77	16.67
0.37	42	55	30.95	62	47.61
0.16	30	40.1	33.67	50	66.67

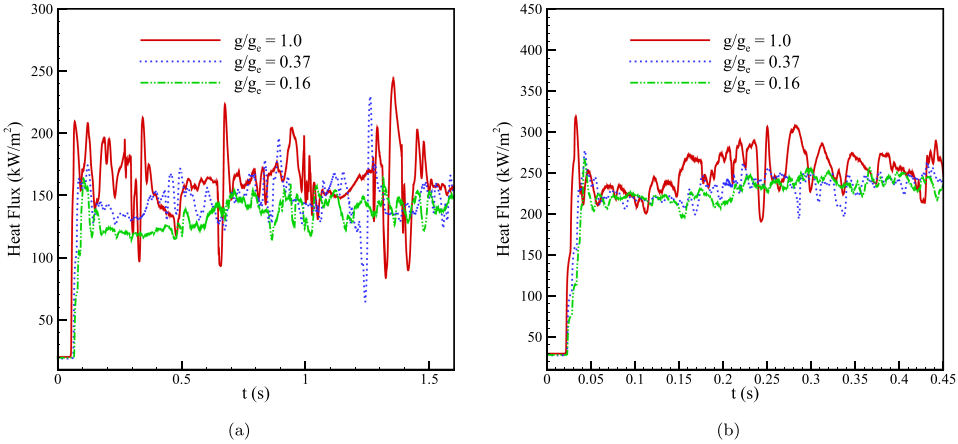

FIG. 13. Variation of heat flux at different gravity levels at an applied electric field intensity of (a) 2×10^5 V/m and (b) 3×10^5 V/m for water at $\Delta T = 5$ K.

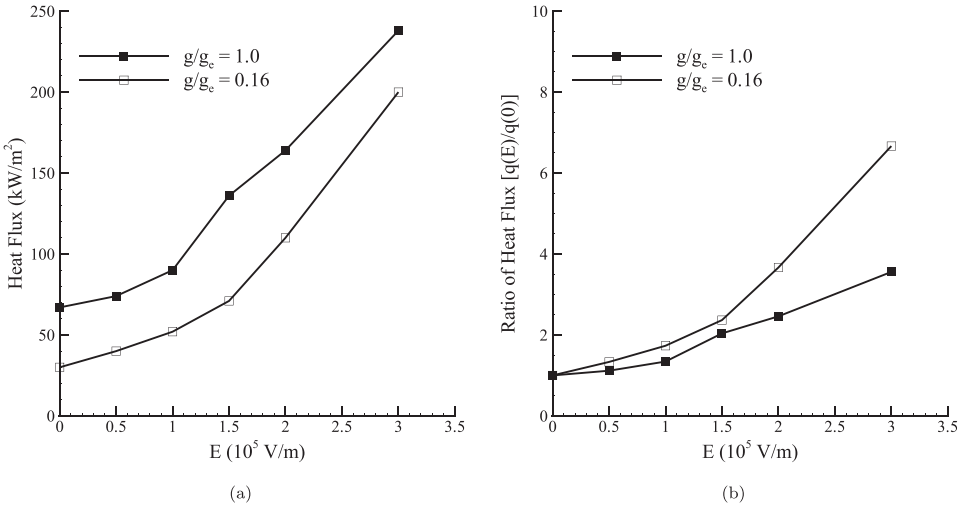

FIG. 14. Variation of (a) heat flux and (b) ratio of heat flux with electric field to that of without electric field in normal and reduced gravity conditions for water at $\Delta T = 5$ K.

of gravity at a specified high intensity (2×10^5 V/m) of electric field tend to become close. At even higher value of electric field (3×10^5 V/m), the heat flux plots almost coincide with each other at different levels of gravity. Under the reduced gravity condition, the magnitude of heat flux is less than under the normal gravity condition at every given intensity of imposed electric field. However, the ratio of heat flux with electric field (q_E) to the heat flux without electric field (q_0) is found to be much larger in the case of reduced gravity condition for the range of applied electric field. This has been illustrated by the plots in Figs. 14(a) and 14(b). It can be observed from the plots in Fig. 14(a) that as the intensity of electric field increases, the difference in heat flux values decreases between normal and reduced gravity conditions. Hence, the dominance of electric field seems to increase with the increase in intensity of electric field for the lower value of gravity.

V. SELF-SIMILARITY DURING BUBBLE GROWTH

Generation of vapour due to applied heat flux results in velocity jump across the liquid-vapour interface. Aggravated

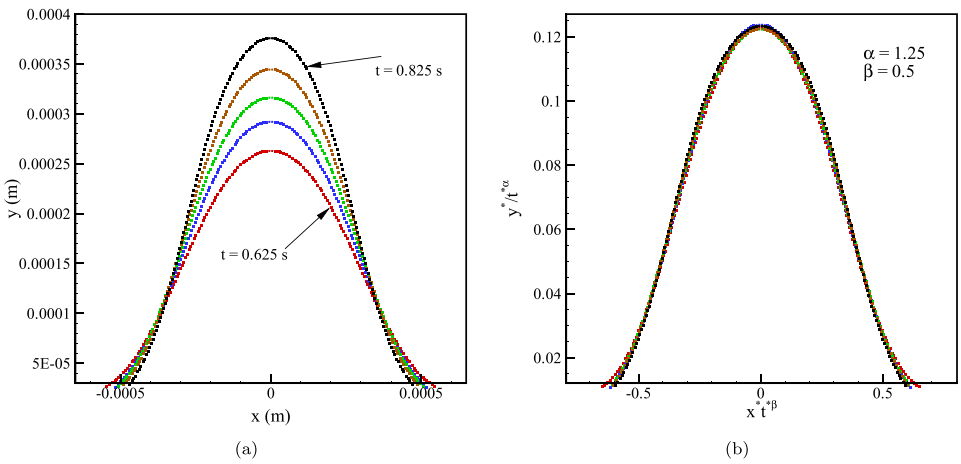

FIG. 15. (a) Interface profiles at different instants of time from t = 0.625 s to t = 0.825 s for $\Delta T = 2$ K. (b) Profiles at the same instants of time as in left hand side, rescaled following $y^*/t^{*\alpha} = ax^*t^{*\beta}$.

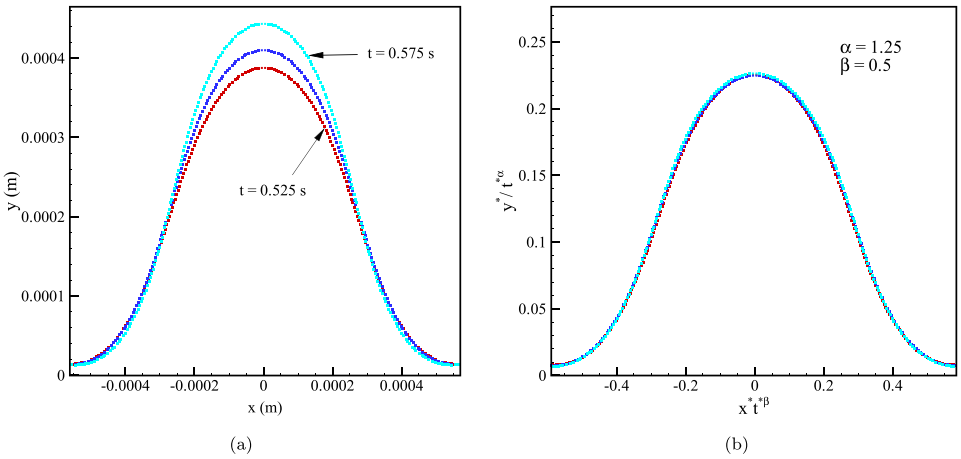

FIG. 16. (a) Interface profiles at different instants of time from t = 0.525 s to t = 0.575 s ΔT = 5 K. (b) Profiles at the same instants of time as in left hand side, rescaled following $y^*/t^{*\alpha} = ax^*t^{*\beta}$.

by the gravity-capillary effects combined with the applied heat flux, it generates free surface waves. The bubble growth is a consequence of increased Rayleigh-Taylor instability at the liquid-vapour interface at lower degree of superheat. The instability mode shifts to Taylor-Helmholtz as the superheat is increased.[37,38] The vapour bulge incipience tending to bubble formation can be considered as a dynamical phenomenon exhibiting singularity. Every physical system exhibiting such singularities leads to an ultraviolet cutoff (defined by Hogrefe *et al.*[51]) terminating the singularity. In this case, this cutoff is depicted as the detachment of the growing bubble from the bulk vapour phase.

The vapour growth affected by the Rayleigh instability leads to a mushroom-like structure in the case of viscous fluids. This phenomenon initiates the neck formation in the growing vapour mass. Duchemin *et al.*[52] studied the self-similarity behaviour of the tip of the growing spikes in accelerated motion of the liquid due to the Rayleigh-Taylor instability. The study assumed inviscid fluid with high density ratio. As mentioned in Hogrefe *et al.*,[51] the instability in the presence of stretching occurring at the neck results due to the axial velocity of the fluid around the growing spike. Hogrefe *et al.*[51] developed a relation for the height of the growing spike in Faraday singularity as a function of the radius of the spike and the time of growth. The profile of the growing spike is given as $y = bt^{\alpha}(xt^{\beta})^{\gamma}$.

Considering the initial phase of bubble growth as influenced by the Rayleigh-Taylor mode of instability, we performed self-similarity analysis of the profiles of growing vapour bubbles. The fitting function we used is of the form $y^*/t^{*\alpha} = ax^*t^{*\beta}$ as the general solution for the kinetic free-surface problem of Hogrefe *et al.*[51] For small superheat value of $\Delta T = 2$ K, between the time instants t = 0.625 s and t = 0.825 s, the growing bubble profiles collapse on a single curve (Fig. 15). The relation between α and β is followed as, $\alpha = 1 + \beta/2$. The value of the constant a is 1 and the values of the exponents α and β are 1.25 and 0.5, respectively. The dimensional quantities are scaled with half of the characteristic wavelength, $\lambda_B/2$ and the time is scaled using viscous time, $\tau_v = l^2\rho_l/\mu_l$ where l is the characteristic length scale. The same analysis is performed at ΔT = 5 K for the same values of α and β. The profile is shown in Fig. 16. It is observed that the growing vapour bubble profiles follow self-similarity but for a smaller time range, i.e., between t = 0.525 s and t = 0.575 s. This indicates the variation in the values of exponents α and β with the increase in the value of the superheat. The above indication proved to be valid from the self-similarity profiles of interface growth at ΔT = 10 K as shown in Fig. 17. The values of the exponents are taken as α = 6.4 and β = 4.5 and the relation between α and β is $\alpha = 1 + 6\beta/5$. The difference in the values of the scaling exponents and their inter-relationship can be attributed to the change in instability mode with increasing superheat.

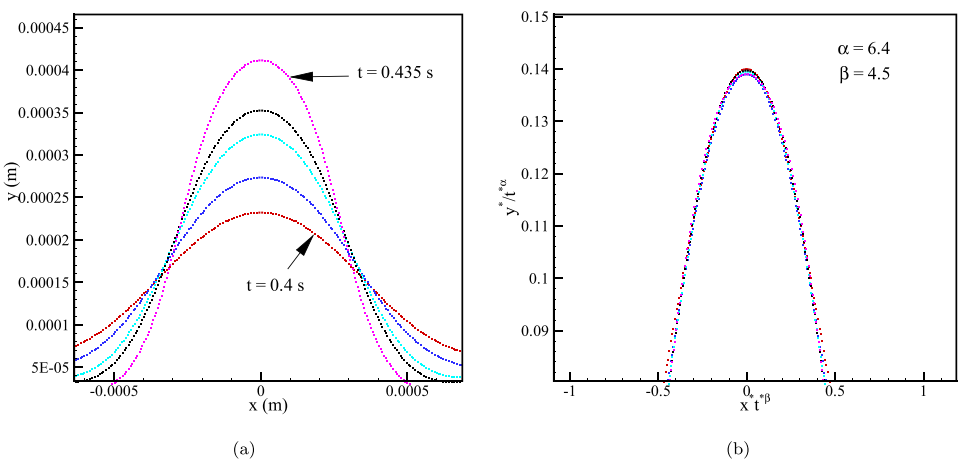

FIG. 17. (a) Interface profiles at different instants of time from t = 0.40 s to t = 0.435 s ΔT = 10 K. (b) Profiles at the same instants of time as in left hand side, rescaled following $y^*/t^{*\alpha} = ax^*t^{*\beta}$.

VI. CONCLUSIONS

From the present analysis based on the direct numerical simulation of saturated film boiling at various gravity levels, it is found that with the reduction in gravity level, the length and time scales of the boiling phenomena increase substantially. The bubble size and height in reduced gravity level are much larger than those of the normal gravity level. The heat transfer rate is deteriorated as the gravity-level decreases. The inclusion of electric field in reduced gravity restores the value of heat flux commensurate with the normal gravity condition. The imposed electric field also reduces the separation distance between adjacent bubble formation sites and the frequency of bubble release is increased. Thus, the application of electric field can be considered as a strategic technique to enhance or control the heat transfer rate under the reduced gravity conditions.

Comparative study of the effect of gravity-level on the film boiling phenomena with an imposed electric field intensity shows that the dominance of electric field on the process enhances with the reduction in gravity. This has been observed from the morphological changes (lateral merger of the bubbles) and the heat transfer characteristics. The percentage change in heat flux due to imposed electric field is observed to increase with the reduction in gravity.

The study of interface profile during the bubble growth period showed that the bubble profiles at different instants of time tend to overlap with each other if a proper scaling law is defined for length and time. The values of the scaling exponents depend on the degree of superheat as the governing instability mode changes with the superheat value. The interface thus exhibits the self-similarity behaviour during the linear stage of bubble growth.

[1] T. Oka, Y. Abe, Y. H. Mori, and A. Nagashima, "Pool boiling of n-pentane, CFC-113, and water under reduced gravity: Parabolic flight experiments with a transparent heater," J. Heat Transfer **117**, 408–417 (1995).

[2] M. Zell, J. Straub, and B. Vogel, "Pool boiling under microgravity," PCH, PhysicoChem. Hydrodyn. **11**, 813–823 (1989).

[3] T. Oka, Y. Abe, K. Tanaka, Y. H. Mori, and A. Nagashima, "Observational study of pool boiling under microgravity," JSME Int. J., Ser. II **35**, 280–286 (1992).

[4] J. H. Lienhard, "On the two regimes of nucleate boiling," J. Heat Transfer **107**, 262–264 (1985).

[5] R. Moissis and P. J. Berenson, "On the hydrodynamic transitions in nucleate boiling," J. Heat Transfer **85**, 221–226 (1963).

[6] R. Siegel and C. Usiskin, "A photographic study of boiling in the absence of gravity," J. Heat Transfer, Trans. ASME, Series C **81**, 230–236 (1959).

[7] C. Usiskin and R. Siegel, "An experimental study of boiling in reduced and zero gravity fields," J. Heat Transfer **83**, 243–253 (1961).

[8] R. Siegel and E. G. Keshock, "Effects of reduced gravity on nucleate boiling bubble dynamics in saturated water," AIChE J. **10**, 509–517 (1964).

[9] H. Merte, Jr. and J. A. Clark, "Boiling heat transfer with cryogenic fluids at standard, fractional, and near-zero gravity," J. Heat Transfer **86**, 351–358 (1964).

[10] H. S. Lee, H. Merte, Jr., and F. Chiaramonte, "Pool boiling curve in microgravity," J. Thermophys. Heat Transfer **11**, 216–222 (1997).

[11] J. Kim and J. F. Benton, "Highly subcooled pool boiling heat transfer at various gravity levels," Int. J. Heat Fluid Flow **23**, 497–508 (2002).

[12] R. Raj, J. Kim, and J. McQuillen, "Subcooled pool boiling in variable gravity environments," J. Heat Transfer **131**, 091502 (2009).

[13] J. Straub, "The role of surface tension for two-phase heat and mass transfer in the absence of gravity," Exp. Therm. Fluid Sci. **9**, 253–273 (1994).

[14] J. Straub, "Microscale boiling heat transfer under 0g and 1g conditions," Int. J. Therm. Sci. **39**, 490–497 (2000).

[15] R. Marek and J. Straub, "The origin of thermocapillary convection in subcooled nucleate pool boiling," Int. J. Heat Mass Transfer **44**, 619–632 (2001).

[16] D. P. Shatto and G. Peterson, "Pool boiling critical heat flux in reduced gravity," J. Heat Transfer **121**, 865–873 (1999).

[17] D. M. Qiu, V. K. Dhir, D. Chao, M. M. Hasan, E. Neumann, G. Yee, and A. Birchenough, "Single-bubble dynamics during pool boiling under low gravity conditions," J. Thermophys. Heat Transfer **16**, 336–345 (2002).

[18] H. S. Abarajith, V. K. Dhir, and G. Son, "Numerical simulation of the dynamics of multiple bubble merger during pool boiling under reduced gravity conditions," in Proceedings of 7th Japan-US Seminar on Two-Phase Flow Dynamics, Moriyama, Japan, 2004.

[19] V. K. Dhir, G. R. Warrier, E. Aktinol, D. Chao, J. Eggers, W. Sheredy, and W. Booth, "Nucleate pool boiling experiments (NPBX) on the international space station," Microgravity Sci. Technol. **24**, 307–325 (2012).

[20] E. Aktinol, G. R. Warrier, and V. K. Dhir, "Single bubble dynamics under microgravity conditions in the presence of dissolved gas in the liquid," Int. J. Heat Mass Transfer **79**, 251–268 (2014).

[21] G. R. Warrier, V. K. Dhir, and D. F. Chao, "Nucleate pool boiling experiment (NPBX) in microgravity: International Space Station," Int. J. Heat Mass Transfer **83**, 781–798 (2015).

[22] S. X. Wan and J. F. Zhao, "Pool boiling in microgravity: Recent results and perspectives for the project DEPA-SJ10," Microgravity Sci. Technol. **20**, 219–224 (2008).

[23] J. F. Zhao, J. Li, N. Yan, and S. F. Wang, "Bubble behavior and heat transfer in quasi-steady pool boiling in microgravity," Microgravity Sci. Technol. **21**, 175–183 (2009).

[24] F. M. Verplaetsen and J. A. Berghmans, "The influence of an electric field on the heat transfer rate during film boiling of stagnant fluids," Rev. Gen. Therm. **37**, 83–88 (1997).

[25] F. M. Verplaetsen and J. A. Berghmans, "Film boiling of an electrically insulating fluid in the presence of an electric field," Heat Mass Transfer **35**, 235–241 (1999).

[26] P. Di Marco and W. Grassi, "Motivation and results of a long-term research on pool boiling heat transfer in low gravity," Int. J. Therm. Sci. **41**, 567–585 (2002).

[27] P. Carrica, P. Di Marco, and W. Grassi, "Electric field effects on film boiling on a wire," Exp. Heat Transfer **9**, 11–27 (1996).

[28] R. L. Johnson, "Effect of an electric field on boiling heat transfer," AIAA J. **6**, 1456–1460 (1968).

[29] P. Di Marco, W. Grassi, and F. Trentavizi, "Pool film boiling experiments on a wire in low gravity," Ann. N. Y. Acad. Sci. **974**, 428–446 (2001).

[30] M. Markels and R. L. Durfee, "The effect of applied voltage on boiling heat transfer," AIChE J. **10**, 106–110 (1964).

[31] R. F. Lovenguth and D. Hanesian, "Boiling heat transfer in the presence of nonuniform, direct current electric fields," Ind. Eng. Chem. Fundam. **10**, 570–576 (1971).

[32] P. Cooper, "EHD enhancement of nucleate boiling," J. Heat Transfer **112**, 458–464 (1990).

[33] G. Son and V. K. Dhir, "Numerical simulation of saturated film boiling on a horizontal surface," J. Heat Transfer **119**, 525–533 (1997).

[34] G. Son and V. K. Dhir, "Numerical simulation of film boiling near critical pressures with a level set method," J. Heat Transfer **120**, 183–192 (1998).

[35] D. Gerlach, G. Tomar, G. Biswas, and F. Durst, "Comparison of volume-of-fluid methods for surface tension-dominant two-phase flows," Int. J. Heat Mass Transfer **49**, 740–754 (2006).

[36] G. Tomar, G. Biswas, A. Sharma, and A. Agrawal, "Numerical simulation of bubble growth in film boiling using a coupled level-set and volume-of-fluid method," Phys. Fluids **17**, 112103 (2005).

[37] G. Tomar, G. Biswas, A. Sharma, and S. W. Welch, "Multimode analysis of bubble growth in saturated film boiling," Phys. Fluids **20**, 092101 (2008).

[38] A. Hens, G. Biswas, and S. De, "Analysis of interfacial instability and multimode bubble formation in saturated boiling using coupled level set and volume-of-fluid approach," Phys. Fluids **26**, 012105 (2014).

[39] S. W. J. Welch and G. Biswas, "Direct simulation of film boiling including electrohydrodynamic forces," Phys. Fluids **19**, 012106 (2007).

[40] G. Tomar, G. Biswas, A. Sharma, and S. W. J. Welch, "Influence of electric field on saturated film boiling," Phys. Fluids **21**, 032107 (2009).

[41] G. Tomar, D. Gerlach, G. Biswas, N. Alleborn, A. Sharma, F. Durst, S. Welch, and A. Delgado, "Two-phase electrohydrodynamic simulations using a volume-of-fluid approach," J. Comput. Phys. **227**, 1267–1285 (2007).

[42]V. Pandey, G. Biswas, and A. Dalal, "Effect of superheat and electric field on saturated film boiling," Phys. Fluids **28**, 052102 (2016).
[43]J. U. Brackbill, D. B. Kothe, and C. Zemach, "A continuum method for modeling surface tension," J. Comput. Phys. **100**, 335–354 (1992).
[44]V. Pandey, A. Dalal, and G. Biswas, "Bubble formation in film boiling including electrohydrodynamic forces," Procedia IUTAM **15**, 86–94 (2015).
[45]V. Pandey, A. Dalal, G. Biswas, and G. Natarajan, "Effect of electrohydrodynamics in saturated film boiling with varying superheat," in ICHMT Digital Library Online (Begel House, Inc., 2015).
[46]D. K. Agarwal, S. W. J. Welch, G. Biswas, and F. Durst, "Planar simulation of bubble growth in film boiling in near-critical water using a variant of the VOF method," J. Heat Transfer **126**, 329–338 (2004).
[47]P. J. Berenson, "Film boiling heat transfer from a horizontal surface," J. Heat Transfer **83**, 351–356 (1961).
[48]B. P. Leonard, "A stable and accurate convective modelling procedure based on quadratic upstream interpolation," Comput. Methods Appl. Mech. Eng. **19**, 59–98 (1979).
[49]E. G. Puckett, A. S. Almgren, J. B. Bell, D. L. Marcus, and W. J. Rider, "A high-order projection method for tracking fluid interfaces in variable density incompressible flows," J. Comput. Phys. **130**, 269–282 (1997).
[50]Y. C. Chang, T. Y. Hou, B. Meriman, and S. Osher, "A level set formulation of Eulerian interface capturing methods for incompressible fluid flows," J. Comput. Phys. **124**, 449–464 (1996).
[51]J. E. Hogrefe, N. L. Peffley, C. L. Goodridge, W. T. Shi, H. G. E. Hentschel, and D. P. Lathrop, "Power-law singularities in gravity-capillary waves," Phys. D: Nonlinear Phenom. **123**, 183–205 (1998).
[52]L. Duchemin, C. Josserand, and P. Clavin, "Asymptotic behavior of the Rayleigh-Taylor instability," Phys. Rev. Lett. **94**, 224501 (2005).